https://doi.org/10.5194/angeo-2020-66
Preprint. Discussion started: 16 October 2020

Annales Geophysicae Discussions

Warm protons at comet 67P/Churyumov-Gerasimenko – Implications for the infant bow shock

Charlotte Goetz[1,2], Herbert Gunell[3,4], Fredrik Johansson[5], Kristie LLera[6], Hans Nilsson[7], Karl-Heinz Glassmeier[2], and Matthew G. G. T. Taylor[1]

[1]European Space Research and Technology Centre, European Space Agency, Keplerlaan 1, 2201AZ Noordwijk, The Netherlands
[2]Institut für Geophysik und extraterrestrische Physik, Technische Universität Braunschweig, Mendelssohnstr. 3, 38106 Braunschweig, Germany
[3]Department of Physics, Umeå University, 901 87 Umeå, Sweden
[4]Royal Belgian Institute for Space Aeronomy (BIRA-IASB), Avenue Circulaire 3, 1180 Brussels, Belgium
[5]Institutet för Rymdfysik, Lägerhyddsvägen 1, Uppsala, Sweden
[6]Southwest Research Institute, 6220 Culebra Road, San Antonio, TX 78238-5166, USA
[7]Institutet för rymdfysik, Rymdcampus 1, Kiruna, Sweden

Correspondence: Charlotte Goetz (charlotte.goetz@esa.int)

Abstract. Multiple plasma boundaries have been observed at comet 67P/Churyumov-Gerasimenko. Among them was an infant bow shock, an asymmetric structure in the plasma environment that separates the less disturbed solar wind from a plasma with warmer, slower protons. Rosetta crossings of the infant bow shock have so far only been reported for two days. Here, we aim to investigate this phenomenon further by focusing on the proton behaviour and surveying all of the Rosetta comet phase data. We find over 300 events that match the proton signatures at the infant bow shock. We investigate the properties of the plasma and magnetic field at this boundary and the location where it can be found. We find that the protons are preferentially detected at intermediate gas production rates with a slight trend towards larger cometocentric distances for higher gas production rates. The events can mostly be found in the positive convective electric field hemisphere. Both results agree well with simulations of the infant bow shock. The properties of the plasma are harder to constrain, but there is a trend towards higher electron flux, lower magnetic field, higher magnetic field power spectral density, and higher density in the region that contains the warm protons. This is in partial agreement with the previous IBS definitions, however it also indicates that the plasma and this structure are highly non-stationary. For future research, Comet Interceptor, with its multi-point measurements, can help to disentangle the spatial and temporal effects and give more clarity on the influence of changing upstream conditions on the movement of boundaries in this unusual environment.

https://doi.org/10.5194/angeo-2020-66
Preprint. Discussion started: 16 October 2020

Annales Geophysicae Discussions

1 Introduction

The plasma around comet 67P/Churyumov-Gerasimenko (67P) has been explored in depth by the instruments on board the European Space Agency's Rosetta mission (Glassmeier et al., 2007a). The Rosetta orbiter (referred to as *Rosetta* from here on) arrived at the comet in August 2014 and was passivated and impacted the surface in September 2016. The long duration of the mission enables us to explore different stages in the interaction between a comet and the solar wind. As a comet moves from aphelion to perihelion, this interaction evolves from an almost asteroid like interaction regime with very low neutral gas production to one where a fully formed bow shock and diamagnetic cavity are formed (e. g. Glassmeier, 2017; Goetz et al., 2017; Nilsson et al., 2017) along with a plethora of other identified boundaries (Mandt et al., 2016). For a more thorough review of the plasma environment of comets see Götz et al. (2019).

As a comet approaches the Sun, energy input into the surface increases and with it the amount of ice that is sublimated and escapes into space. The neutral gases, mostly water and carbondioxide, undergo photoionisation or electron impact ionisation and form a cloud of heavy ions around the comet (Hässig et al., 2015). As this cloud encounters the solar wind, the cometary ions are accelerated by the convective electric field and eventually assimilated into the solar wind flow. This process of mass-loading results in a deceleration and deflection of the solar wind in the vicinity of the comet.

Biermann et al. (1967) find that the addition of mass can be described as a source term in the mass conservation equation of a fluid description of the plasma. More recently, hybrid simulations or multi-fluid simulations have been the tool of choice to model this environment, because the large ion gyroradii of the cometary ions cannot be accurately described in a single-fluid or MHD approach. This is especially important for comet 67P, where ion gyroradii can be greater than $10000\,\mathrm{km}$ whereas the plasma cloud around the comet is restricted to radii smaller than $1000\,\mathrm{km}$ (see e.g. Koenders et al., 2016b). In this regime the cometary ions are accelerated by the convective electric field far upstream of the comet and a polarisation and ambipolar electric field closer to the nucleus (Nilsson et al., 2018; Gunell et al., 2019). The presence of the convective electric field induces an asymmetry in the interaction region that has consequences for all plasma parameters (Koenders et al., 2016a, b; Edberg et al., 2019).

At higher gas production rates this asymmetry is less pronounced and the influence of the cometary ion gyroradius is diminished, because the magnetic field pile-up at the comet results in higher field magnitudes and thus lower gyroradii. In the classical fluid description by Biermann et al. (1967) and Flammer and Mendis (1991), the mass-loading of the solar wind flow results in a deceleration until a critical point is reached and no mass can be added. A cometary number density of just a few percent is sufficient here, so the critical point is reached already far upstream of the nucleus. There, the interaction between the solar wind and the comet cannot be described by mass-loading alone, instead the flow changes from supersonic to subsonic and a bow shock forms. This prediction is shown to fit well with observations at e. g. comet Halley (Neubauer et al., 1986). The shock itself forms by waves steepening into the nonlinear regime. The speed of the steepened wave is faster than that of the linear wave, but steepening is counteracted by dissipation. If an obstacle and a plasma are in relative motion faster than the speed of linear waves, the waves steepen until an equilibrium is reached where the shock becomes a stationary wave in the obstacle, in this case the comet's, frame of reference (Balogh and Treumann, 2013).

https://doi.org/10.5194/angeo-2020-66
Preprint. Discussion started: 16 October 2020


Annales Geophysicae Discussions

Koenders et al. (2013) compare the bow shock distances from a simple single-fluid model with distances gained from Hybrid simulations and find that the fluid models predicted consistently higher stand off distances. Thus, the ion gyroradius effects are pronounced even in the most fluid-like stage of the plasma around comet 67P.

Bow shocks have been studied at comets (Simon Wedlund et al., 2017) and elsewhere in the solar system (see e. g. Martinecz et al., 2008; Fahr and Siewert, 2015; Hall et al., 2016), but so far the development of a bow shock could not be observed, simply because a bow shock had already been fully formed. Comets provide an excellent laboratory to investigate the process of bow shock formation, where the gradual increase in gas production rate over weeks or months means that the intermediate stages of this interaction can be observed and studied.

The pre-cursor of a bow shock, the infant bow shock (IBS), was first first reported by Gunell et al. (2018). They show two cases from different days of fast changes in the cometary plasma and associate these changes to an asymmetric structure in the solar wind flow that is also found in Hybrid simulations. To detect the IBS the authors look for a change in the magnetic field direction. This ensures that the IBS moves over the spacecraft fairly quickly and the boundary is clearly detectable. This is necessary as Rosetta has a negligible velocity with respect to the boundary. From two days of data it is found that the magnetic field reversal was coincident with an increase in magnitude and wave activity. At the same time the proton velocity distribution function becomes broader and the bulk velocity decreases. The electron flux and energy increases. These observations are compared with hybrid simulations of the comet at similar gas production rates. While the reversal of the magnetic field is used to insure a fast transition of the bow shock from one side of the comet to the other, the main signature of the infant bow shock is the presence of warm, slow protons. A highly asymmetric boundary is seen in the simulations and the simulated proton spectra are very similar to what is observed by Rosetta. Thus the observations are found to be consistent with the detection of an asymmetric boundary. As this boundary is similar to a bow shock at a fully developed comet, it is termed the infant bow shock. Prior to the first identification of an IBS, it was observed that similar signatures seen easily in the mission could possibly be the result of "the crossing of a plasma boundary" (Edberg et al., 2016).

This work aims to study the warm proton signatures first associated with this infant bow shock, but with a broader scope. We then characterize the plasma changes at the boundary as well as its location and discuss how these signatures are related to the infant bow shock and it's characteristics.

2 Data

2.1 Instruments

For this study we use all sensors of the Rosetta Plasma Consortium (Carr et al., 2007) as well as the neutral gas monitor ROSINA-COPS (Balsiger et al., 2007), which provides the neutral gas density as context for the plasma measurements.

The Ion Composition Analyzer (ICA, Nilsson et al., 2007) can provide mass separated differential energy flux with a temporal resolution of 192 s. The field of view (FoV) is 90° in elevation and 360° in azimuth, but there are some obstructions from the spacecraft. Thus, the solar wind signal is not always detected even when it is present in the plasma. Especially rotations of the spacecraft and of the magnetic field can lead to a loss of the solar wind signature. Such loss in the signature

https://doi.org/10.5194/angeo-2020-66
Preprint. Discussion started: 16 October 2020


Annales Geophysicae Discussions

is typically seen as a drastic reduction in the solar wind flux/density. Often, the signal is then still visible in the RPC-IES instrument. Solar wind densities near the comet also decrease due to significant charge exchange losses (Simon Wedlund et al., 2019). This caused rather low densities in the times when Rosetta was just outside the solar wind ion cavity. The RPC-ICA moments used in this study are integrations of the RPC-ICA PSA L4 PHYS-MASS data set, also delivered to the planetary science archive (PSA) as RPC-ICA L5 MOMENT data set. We chose to use the mean proton speed $v_{m,H}$ derived from this data set for assessment of the speed near the IBS. This value is derived by calculating the mean velocity of the proton energy distribution and thus is a more suitable parameter than the 3D velocity moment which is heavily influenced by the pitch angle distribution of the protons (Behar et al., 2017). Here, we only use values for which the density of the protons (calculated from the flux) is above $0.005\,\mathrm{cm}^{-3}$ which is the case for about 90% of all values.

The Ion and Electron Sensor (IES, Burch et al., 2007) provides differential energy flux for electrons and ions (without mass resolution). Its FoV is partially complementary to ICA, but the time resolution is at least $256\,\mathrm{s}$. The measurements at low energies are disturbed by the spacecraft potential, which is between $0\,\mathrm{V}$ and $-20\,\mathrm{V}$ most of the time. For a quantitative analysis of the electron flux, we use the method detailed in Lavraud and Larson (2016) to correct the fluxes and energy bins for the spacecraft potential. We also calculate the flux at $60\,\mathrm{eV}$, and $120\,\mathrm{eV}$ as a time series for the statistical study.

The LAngmuir Probe instrument (LAP, Eriksson et al., 2007) and the Mutual Impedance Probe (MIP, Trotignon et al., 2007) are used to provide plasma density estimates (see e.g. Breuillard et al., 2019, Johansson et al., manuscript in preparation) and measurements of the spacecraft potential (Odelstad et al., 2015). Although the absolute uncertainty of each individual LAP measurement of spacecraft potential may become large (typically 30%) the random noise of the spacecraft potential and the cross-calibrated LAP-MIP density dataset is believed to be only a few percent, and as such suitable for statistical studies.

The magnetic field measurements are provided by the MAGnetometer (MAG, Glassmeier et al., 2007b). Although the maximum sampling rate of the instrument is $20\,\mathrm{Hz}$, only resampled data with $1\,\mathrm{Hz}$ sampling rate is used here, which is sufficient for the study of large scale structures. The magnetic field can only be determined within an accuracy of $\sim 3\,\mathrm{nT}$ per component, due to the influences of spacecraft fields and sensor temperature variations (Goetz et al., 2016, 2017).

2.2 Selection of Intervals

In this study we investigate where and when warm protons are detected near the comet. We aim to identify the regions with warm protons and the boundary that separates the warm and colder proton populations and how the plasma properties react to this boundary. Since we are interested in intervals where Rosetta can still measure the solar wind ions, we do not examine days in which Rosetta was in the solar wind ion cavity (Nilsson et al., 2017), i.e. approximately six months around perihelion (August 2015). All days with characteristics similar to those shown in Gunell et al. (2018) are then flagged. We find 152 days with detections.

To constrain the regions with warm, slow plasma, we then inspect every pre-selected day and set start and end times for each interval in which warm, light ions are detected. This is done according to the following criteria: the solar wind ions measured by ICA and/or IES need to be at significantly lower energies (smaller mean speeds) and show a broader (higher temperature) distribution as compared to surrounding intervals. These are the two criteria used for detection. For verification we evaluate

https://doi.org/10.5194/angeo-2020-66
Preprint. Discussion started: 16 October 2020

Annales Geophysicae Discussions

additional properties like the suprathermal electron fluxes, magnetic field magnitude power spectral density in the frequency range between 50 mHz and 75 mHz and the magnetic field magnitude. However, the direction of change (increase or decrease) is not considered, instead the change in parameters is simply an indicator that the change in proton energy and flux is not due to instrumental or spacecraft effects. The measurements of the electron energy are changing over time as one half of the detector decreases in sensitivity. Thus even small changes in spacecraft attitude or magnetic field direction can have significant consequences in the electron countrate. An additional parameter for characterization is the angle θ, defined by its cosine:

$$\cos(\theta) = \frac{\boldsymbol{E} \cdot \boldsymbol{x}}{|\boldsymbol{E}| \cdot |\boldsymbol{x}|} = \frac{(-\boldsymbol{v} \times \boldsymbol{B}) \cdot \boldsymbol{x}}{|\boldsymbol{v} \times \boldsymbol{B}| \cdot |\boldsymbol{x}|} \tag{1}$$

where $\boldsymbol{x}$ is the spacecraft position in CSEQ, $\boldsymbol{v}$ is the velocity of the undisturbed solar wind and $\boldsymbol{B}$ is the magnetic field. The angle θ was introduced by Gunell et al. (2018) to facilitate a comparison between observations and simulations such as those conducted by Lindkvist et al. (2018). A positive value of the observational $\cos(\theta)$ corresponds to a location in the $+E_c$ hemisphere of simulation space, that is to say, where the coordinate pointing in the same direction as the convective electric field of the solar wind is positive. We also use the sun aspect angles of the spacecraft to exclude an attitude change of the spacecraft as a reason for a change in the proton signal.

This selection is slightly different than the criteria used in Gunell et al. (2018), because we would like to investigate the occurrence of the warm protons regardless of the direction and variability of the magnetic field. Other parameter changes like solar wind velocity and density as well as cometary ion density can also cause warm protons to appear (as stated in previous publications). Thus, limiting the dataset to cases with magnetic field reversals would unnecessarily constrain the number of events.

Event selection was carried out manually rather than automated. Due to the complicated nature of instrument operations by Rosetta, one cannot expect a consistent set of data for all events that could be used in a detection algorithm. For example, a slew of the spacecraft may have rotated the solar wind ions out of the FoV of ICA, meaning that we would not be able to characterize this interval. However, by-eye inspection quickly shows that the solar wind ions are now in the FoV of IES, allowing for a characterization of the event. No combined dataset exists so far. Thus a selection by hand was determined to be the best course of action. For replicability, the list of events with start and end times is given in the supplementary online material.

3 Analysis

From the observations, we identify a total of 370 events where Rosetta observed warm protons. In analogy to the simulation we will refer to the part of the plasma that is warm as the downstream (index d) part of the plasma, while the plasma with more pristine solar wind is referred to as the upstream (index u) region. In some cases, the identification of the downstream plasma is impossible due to data gaps. In this case, the event ends (or begins) at the data gap. As the particle spectra are especially difficult to condense into simple scalar parameters that are statistically representative of a large dataset, we start by examining a subset of 13 events in Sect. 3.1. This is complemented by a statistical treatment of some quantities derived from the whole dataset in Sect. 3.2.

https://doi.org/10.5194/angeo-2020-66
Preprint. Discussion started: 16 October 2020

Annales Geophysicae Discussions
Open Access
EGU

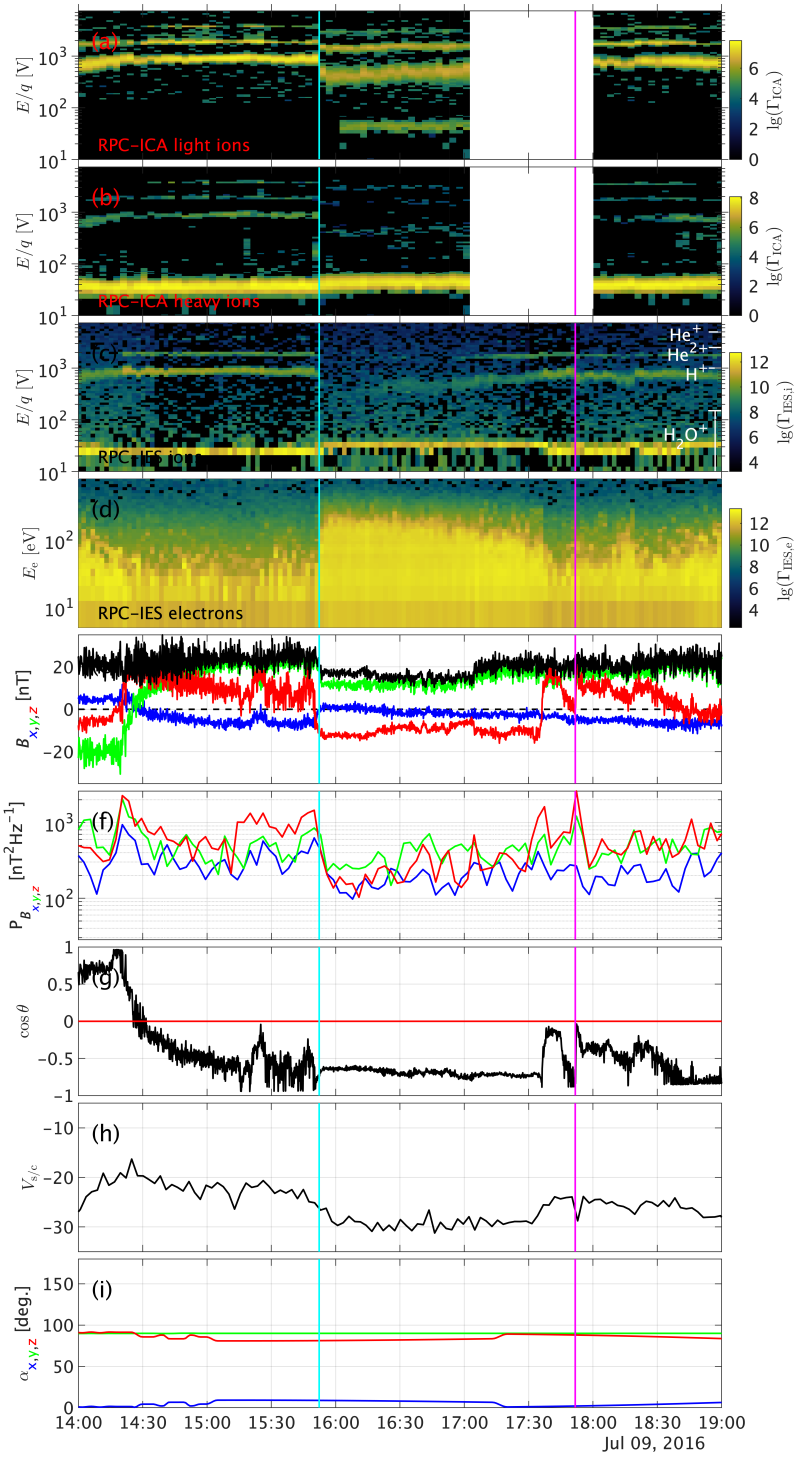

Figure 1. Observations of the event on July 9th, 2016. From top to bottom: a) ICA solar wind ions, b) ICA heavy ions, c) IES ions, d) IES electrons, e) magnetic field in CSEQ coordinates, f) magnetic power spectral density in the frequency range between 2 mHz and 15 mHz, g) angle between spacecraft position and convective electric field, h) spacecraft potential, and i) attitude.

https://doi.org/10.5194/angeo-2020-66
Preprint. Discussion started: 16 October 2020

Annales Geophysicae Discussions
Open Access
EGU

Start time	H^+ E/q	$\Gamma_{IES,e}$	B_m	P_B	cos(θ)	$V_{s/c}$	H^+ E/q	$\Gamma_{IES,e}$	B_m	P_B	cos(θ)	$V_{s/c}$
Dec 07, 14 03:49	↓	↑	↓	↓	–	–	↑	–	–	–	–	–
Dec 25, 14 09:50	↓	↑	↓	↓	–		↑	↓	–	–	–	
Jan 04, 15 12:19	↓	↑	–	↓	–		↑	–	–	↑	–	
Jan 04, 15 19:55	↓	↑	↑	–	–		↑	↓	↑	–	↓	
Mar 07, 15 05:48	↓	↑	↑	↑	↑		↑	↑	↓	–	↓	
Feb 10, 16 09:02							↑	↓	↓	↓	↓	↓
Feb 26, 16 05:50	↓	–	–	–	–	–	↑	–	↓	–	↓	–
Feb 29, 16 00:27	↓	–	–	–	↓	–	↑	↓	↓	↓	↑	–
Apr 08, 16 03:27	↓	↑	↓	↓	↑	↓	↑	↓	↑	↑	↓	↑
Apr 08, 16 07:58	↓	↑	↓	↑	–	↓	↑	↓	↑	–	↓	↑
Jun 01, 16 12:11	↓	↑	↑	↑	↑	–						
Jul 09, 16 12:43	↓	↑	↑	↑	–	↓	↑	↓	–	–	↓	↓
Jul 09, 16 15:52	↓	↑	↓	↓	–	↓	↑	↓	–	–	↑	↑
Median	↓	↑	–	–	–	– ↓	↑	↓	–	–	↓	–

Table 1. List of 13 events chosen for a more detailed study and list of parameter changes when crossing from upstream to downstream (inward, left) and from downstream to upstream (outward, right). The last line summarizes events by giving a median change. Missing signs indicate that no data was available.

3.1 Detailed investigation of a small subset of events

We begin with a detailed investigation of a smaller subset of events. These events were chosen somewhat arbitrarily, so as to represent a broad picture of the situation, however emphasis was put on events that were easily visible for illustration purposes. Thus, we have chosen 13 events, as listed in Table 1.

Fig. 1 shows one example event, observations for the other events can be found in the appendix (Fig. A1 and A2). The blue line indicates the time when Rosetta passed from the upstream to the downstream region, the magenta line shows the outbound pass. From top to bottom: we see a pronounced decrease in the proton energy as well as a broadening of the energy band in the downstream region. This was the criterion of selection for the events. The energy of the heavy ions (panel b) is increased slightly. The IES signal of the protons (panel c) is lost at first, but then the protons return to the field of view and appear broader and slower. The IES electron signature (panel d) increases in energy and flux. Interestingly, the flux diminishes at the same time that the proton energy increases gradually. The magnetic field (panel e) decreases in magnitude and the z-component changes sign. The power spectral density of the magnetic field (panel f) is decreased. The angle θ does not change significantly (panel g), but the magnetic field direction does change. This is because θ represents the angle between the x-axis and magnetic field, thus it does not reflect changes in the z-component of the magnetic field very well. The spacecraft potential (panel h) is lower in the downstream region. We use this as a proxy for the density of the plasma: the lower the spacecraft potential, the higher the density. Thus the density is higher in the downstream region. We also ensure that these changes in the particle signatures

https://doi.org/10.5194/angeo-2020-66
Preprint. Discussion started: 16 October 2020

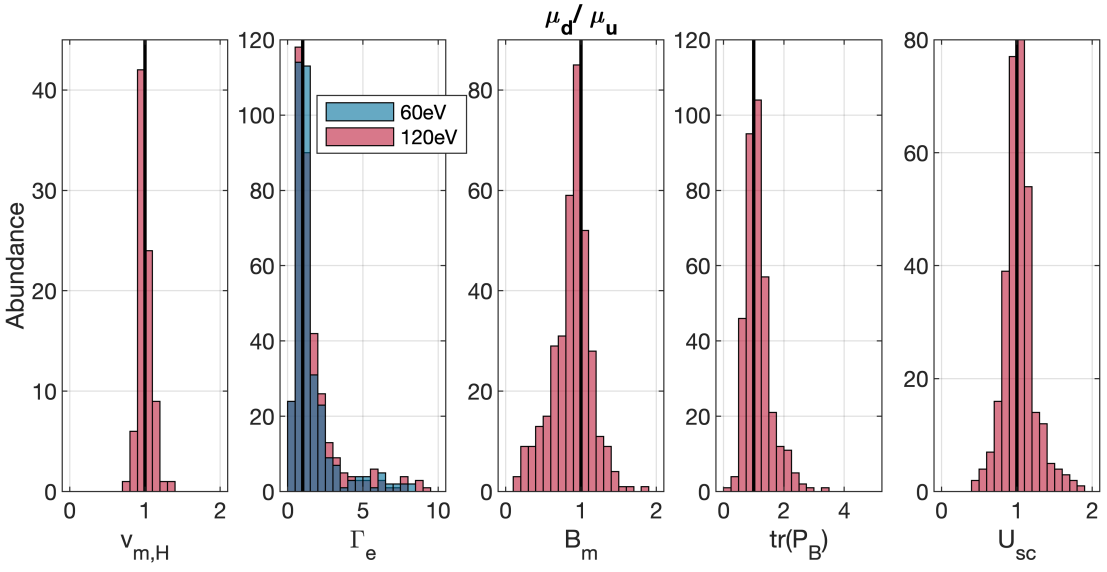

Figure 2. Comparison of the upstream and downstream mean values for five of the six parameters chosen for investigation.

are not due to a change in FoV, thus we included the spacecraft attitude (panel i) to confirm that it only changes insignificantly in the time interval in question. For this initial study we have categorized the change at the two boundary regions for all 13 events. Since no data is available for the outbound pass for one event and for the inbound pass for one event, we have a total of 12 events for each the inbound and outbound pass. The parameters that we use to characterize how the plasma changes at the boundary are the proton energy H^+ E/q, the flux of the electrons $\Gamma_{IES,e}$, the magnetic field magnitude B_m, the power spectral density of the magnetic field P_B, the angle $\cos(\theta)$, and the spacecraft potential $V_{s/c}$. The changes are indicated in Table 1.

Since the proton energy was used as a selection criterion the proton energy in the downstream region is always lower than upstream. For the other parameters, we find that the energy of the electrons is almost always increased and the spacecraft potential is often lower in the downstream region. For the other parameters, no such clear pattern emerges. The magnetic field and magnetic field power spectral density are sometimes increased, sometimes decreased, with no apparent pattern. The angle of the field can change, but events without field changes also exist. It is also interesting to note that not all events have a sharp boundary. For example, the event on Feb 10th, 2016 (Fig. A1, bottom right) shows that the transition can sometimes be very broad. We see that it takes about 20 minutes for the magnetic field to change direction, and for the proton flux to gradually increase in width and decrease in energy. The beginning and end of this transition period are marked with two lines, both magenta in colour.

3.2 A statistical study of the entire event dataset

Here, we expand the discussion to the entire dataset of 370 events.

https://doi.org/10.5194/angeo-2020-66
Preprint. Discussion started: 16 October 2020

Annales Geophysicae Discussions

We investigate the behaviour of the same parameters as above, but now for all events. The statistical assessment of the proton flux is complicated by an incomplete FoV and the broad distribution of the protons. Therefore, moments of the distribution function are less representative in the situation at comet 67P. Instead, we use the mean speed of the protons: a simple 1D approximation of the energy spectra of the protons. This parameter does not represent the angular spread of the particles, but it is the most representative of the energy vs. time spectrograms that we used to identify events. Even this parameter is not always reliable, as it only uses ICA spectra and some events that were identified earlier are only (better) visible in the IES spectra. To assess the electron flux changes, we chose two energy values (60 eV and 120 eV) to extract a 1D time series of the flux at these energies. They were chosen based on an inspection of the subset of events, were these energy bands showed the clearest change. But we should also bear in mind that the IES electron detector decreased in sensitivity in the latter half of 2015 (Madanian et al., 2020), thus electron fluxes may be below the noise level quite often, especially in 2016. We have not included the angle θ in this investigation, because the angle of the field is very susceptible to magnetometer offset problems, especially for low field regimes and requires a visual inspection that is not possible for a statistical study.

Figure 2 shows histograms of the ratio of the downstream to the upstream mean parameters μ_d/μ_u. To calculate this ratio we use an interval of 18 minutes before and after the event, as well as all the observations of the downstream plasma. The interval length was also varied from 10 minutes up to an hour, but the overall results were not impacted by that.

These larger statistics agree mostly with the observations from the 13 events that were categorized by hand. From left to right:

$v_{m,H}$ The proton energy (decrease) and width of the energy spectra (increase) were originally chosen as selection criteria. The downstream to upstream ratio shows a larger number of values below than above unity as expected for a decrease in energy as was seen in Sect. 3.1. However, the mean speed of the protons does not always decrease. This is probably due to the way that the mean speed is calculated, as it is the centre of weight of the energy spectra. For a low signal-to-noise ratio, this value is not meaningful.

Γ_e In our smaller subset, the energy of the electrons in the 60 eV and 120 eV band increases in 10 of the 12 inbound passes and decreases in 8 of the 12 outbound passes. In the entire dataset the electron energy is increased in the downstream region in 60% of all cases. That the larger statistics do not show the same behaviour may in part be because the energy dependent electron flux is difficult to condense to a single parameter, and the instrument sensitivity declined significantly after perihelion. We have observed cases, where the flux was very low and thus changes were not visible.

B_m The magnetic field decreases in 68% of cases. This is consistent with the case studies above.

tr(P_B) The trace power spectral density increases downstream in 58% of all cases.

U_{sc} The spacecraft potential decreases in 52% of all cases. This is consistent with the case studies, where the spacecraft potential was either decreased downstream or not changed at all.

https://doi.org/10.5194/angeo-2020-66
Preprint. Discussion started: 16 October 2020

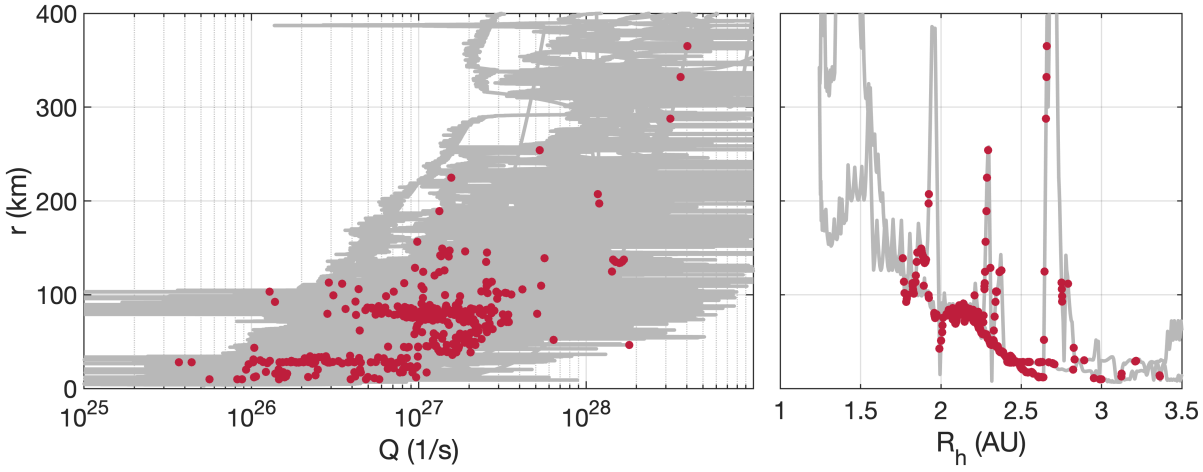

Figure 3. Cometocentric distance of the spacecraft over gas production rate (left) and heliocentric distance (right). The gas production rate was derived from measured neutral gas densities using a spherically symmetric model. The grey lines show the position during the entire Rosetta mission, while the red dots indicate boundary crossings.

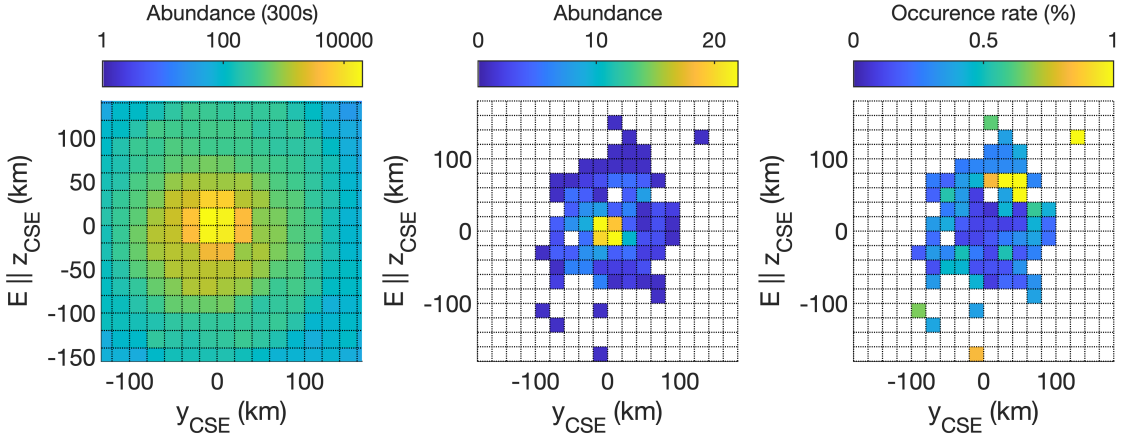

Figure 4. Abundance of the position of the spacecraft (left), position at which warm protons were detected (middle) and occurrence rate of detections normalized to the spacecraft dwell time (right).

https://doi.org/10.5194/angeo-2020-66
Preprint. Discussion started: 16 October 2020


Annales Geophysicae Discussions

3.3 Location of the events

From Gunell et al. (2018) the expectation is that the IBS and the associated warm ions are detected preferentially at the intermediate activity stage of comet 67P. To investigate this, we estimate the gas production rate Q from the in-situ neutral gas density measurements under the assumption of a simple, spherical outgassing model (Haser, 1957).

Figure 3 shows the occurrence location of the events dependent on the outgassing rate and heliocentric distance. To check for observation bias, the trajectory of the spacecraft is indicated in grey. We find that most detections are made between $Q = 10^{26}\,\mathrm{s}^{-1}$ and $Q = 6 \times 10^{27}\,\mathrm{s}^{-1}$, which corresponds roughly to heliocentric distances between 1.7 AU and 2.7 AU. The cometocentric distance of the events increases with increasing gas production rate.

The convective electric field E_c in the solar wind accelerates the cometary ions in only one direction and, to conserve momentum, the solar wind is deflected in the opposite direction (Deca et al., 2017). We transform the position of the events that we identified into a Cometocentric Solar Electric field (CSE) system. Specifically, the z-axis is aligned with $-\boldsymbol{v_{sw}} \times \boldsymbol{B}$, where $\boldsymbol{B}$ is the measured magnetic field at the spacecraft location and $\boldsymbol{v_{sw}}$ is the solar wind velocity. For this comparison, the solar wind direction is simply assumed as the direction away from the Sun. This has been shown to be a good estimator for the CSE system (Edberg et al., 2019). The local solar wind velocity at this stage in the cometary development is not representative of the upstream solar wind direction, because of deflection (Nilsson et al., 2017). This can also be seen in simulations (e. g. Fig. 5), where the deflection of the solar wind ions becomes significant very close to the infant bow shock, exactly in the region that is used for calculation of the electric field direction. Thus a more accurate estimate is impossible as undisturbed solar wind observations are not available at the comet.

The left panel of Fig. 4 shows the location of the spacecraft in this CSE system binned in 300s intervals. There is very good coverage of the entire coma in the terminator plane. We chose to limit our investigation to the $y_{\mathrm{CSE}} - z_{\mathrm{CSE}}$-plane, because Rosetta was for the most time very close to the nucleus in a terminator ($x = 0$) orbit and coverage in the x-direction is insufficient. In the middle panel, the location of the events is shown in the same coordinate system. The right panel shows the occurrence rate of warm proton detections. The most detections are in the ($+y$,$+E_c$) quadrant.

4 Discussion

We have performed a statistical study of periods where Rosetta observed protons with higher temperature and lower mean energy than the solar wind. It is worthwhile to discuss whether all or only a subset of these were observations of an infant bow shock as reported by Gunell et al. (2018).

On average the flux of electrons does increase downstream of the structure, which is in agreement with the properties of the IBS as reported in the previous study. However many events also show an opposite behaviour. The agreement is better in the smaller dataset of 13 cases than in the complete dataset. Thus, at least some of this discrepancy might be attributable to the inability of the flux at 60 eV or 120 eV to accurately represent the electron spectra.

For the power spectral density of the magnetic field one would, for a shock, expect an increase downstream of the shock where oscillations are known to occur. We see this in 58% of the cases of the whole data set, but only in 32% of the cases

https://doi.org/10.5194/angeo-2020-66
Preprint. Discussion started: 16 October 2020

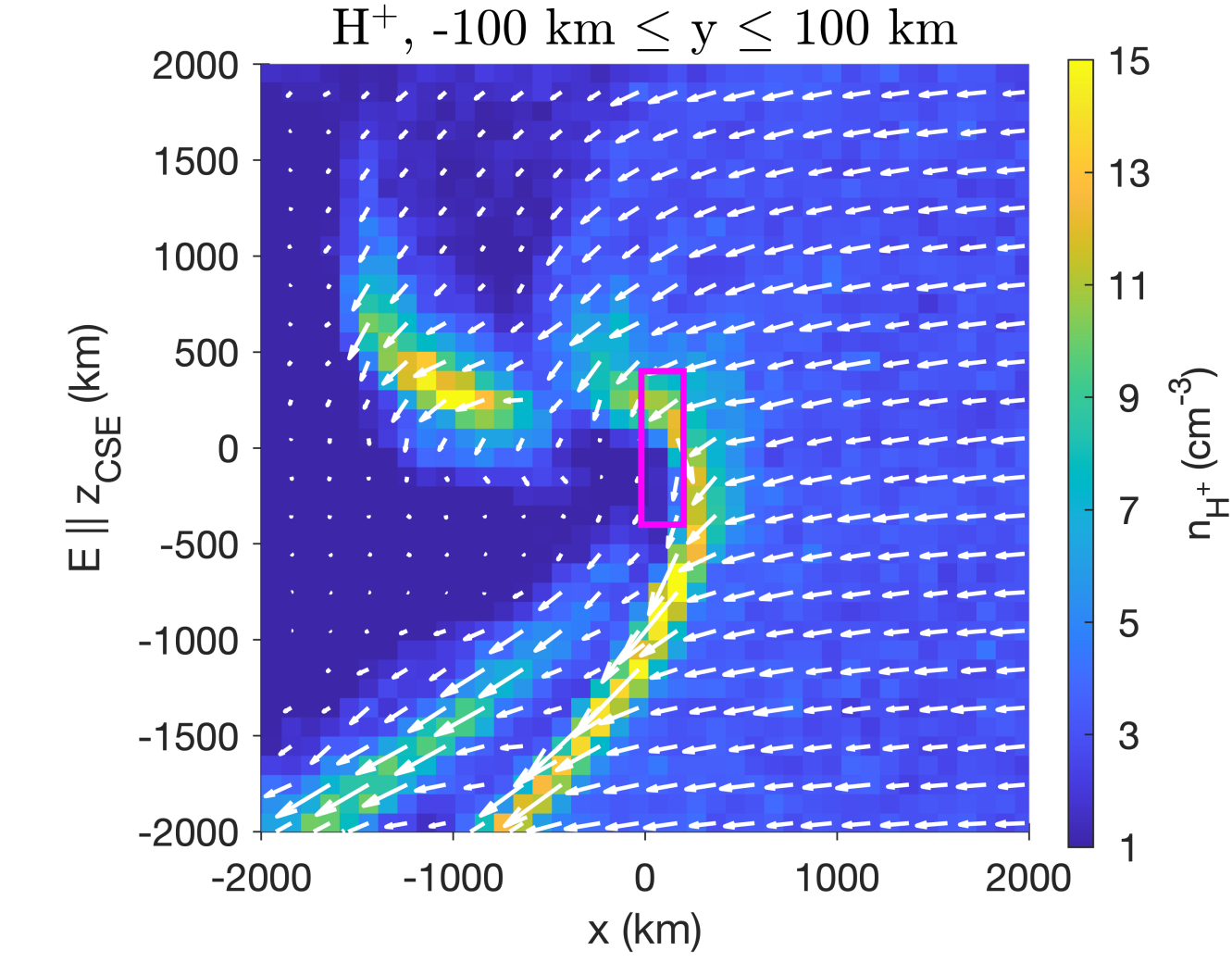

Figure 5. Density and direction of the flux of the protons from the Hybrid simulations. Here, the Sun is to the right.

https://doi.org/10.5194/angeo-2020-66
Preprint. Discussion started: 16 October 2020


Annales Geophysicae Discussions Open Access EGU

in the smaller subset. Although events without an enhanced suprathermal electron flux or increased magnetic power spectral density could be examples of phenomena other than an IBS, it is not necessarily so. The region downstream of a shock is structured. Oscillations are expected to peak close to the shock and decay farther downstream (Ziegler and Schindler, 1988), and also the scale lengths are different for electrons and protons. It is thus possible for the spacecraft to probe only a region with hot protons without passing through regions with hot electrons or large amplitude wave activity. This would mean that the spacecraft probed parts of the equivalent to a planetary magnetosheath, whose properties depend on the presence of a bow shock, but without crossing the bow shock itself. This must at times occur, given the slow motion of the spacecraft of the order of $1\,\mathrm{m\,s^{-1}}$.

As the spacecraft moves very slowly the observations rely on changes in the upstream conditions for the spacecraft to pass from one region to another. Gunell et al. (2018) only showed events where the location of the spacecraft in a convective electric field aligned system changed, which is caused by a change of the direction of the interplanetary magnetic field. In this study, we do not rely on the convective electric field to change (represented by the angle θ). Any change in upstream conditions that moves the boundary can also allow Rosetta to cross it. This gives us access to a larger set of events, but we do not know what upstream condition change lead to the boundary movement. Our observations will therefore be affected not only by the change of one specific solar wind parameter, but also by the correlation between the different solar wind parameters that change together systematically. We have also shown that some events have very broad transitions regions (10s of minutes), a scale over which the plasma has previously been shown to be extremely variable. The behaviour of the magnetic field magnitude is an example of this. In shock modelling, the magnetic field is generally stronger on the downstream than the upstream side of the shock. In our statistics, we have many cases of the opposite behaviour. One possibility is that the solar wind dynamic pressure pushes the IBS further towards the comet and Rosetta passes into the upstream region, but at the same time the magnitude of the interplanetary field increases, resulting in a new, stronger magnetic field. Evidence for such a correlation in the solar wind has been found before (see Fig. 4 of Maggiolo et al., 2017). To separate the behaviour of the solar wind itself from the cometary response to the solar wind one would need an upstream monitor in the vicinity of the comet. Thus, the observations are not inconsistent with the theory of an infant bow shock.

When considering just the subset of events where the plasma behaves as expected for an IBS (the magnetic field increases downstream along with an increase in the power spectral density, increase in electron flux). About 10% of all events fulfil all these criteria and one such event is shown in Fig. 6. Although the ICA data is missing for the first half of the event, we can clearly see warm proton fluxes in the IES data for the first half of the event. For the second half they are registered by ICA. The electron flux, magnetic field magnitude and power spectral density are increased in the region with warm protons. This event is very similar to that shown in Gunell et al. (2018). We therefore conclude that these 10% are definitely the same IBS structure as reported before. For the events that do not comply with these criteria, we have examined if they only occur under specific circumstances (i.e. position, gas production rate, spacecraft potential), but no apparent pattern emerges. There are also no correlations between the changes in field and changes in the electron flux. For the events where the magnetic field increases, the flux of electrons can both increase and decrease. The same goes for the spacecraft potential, as well as the power spectral density.

https://doi.org/10.5194/angeo-2020-66
Preprint. Discussion started: 16 October 2020

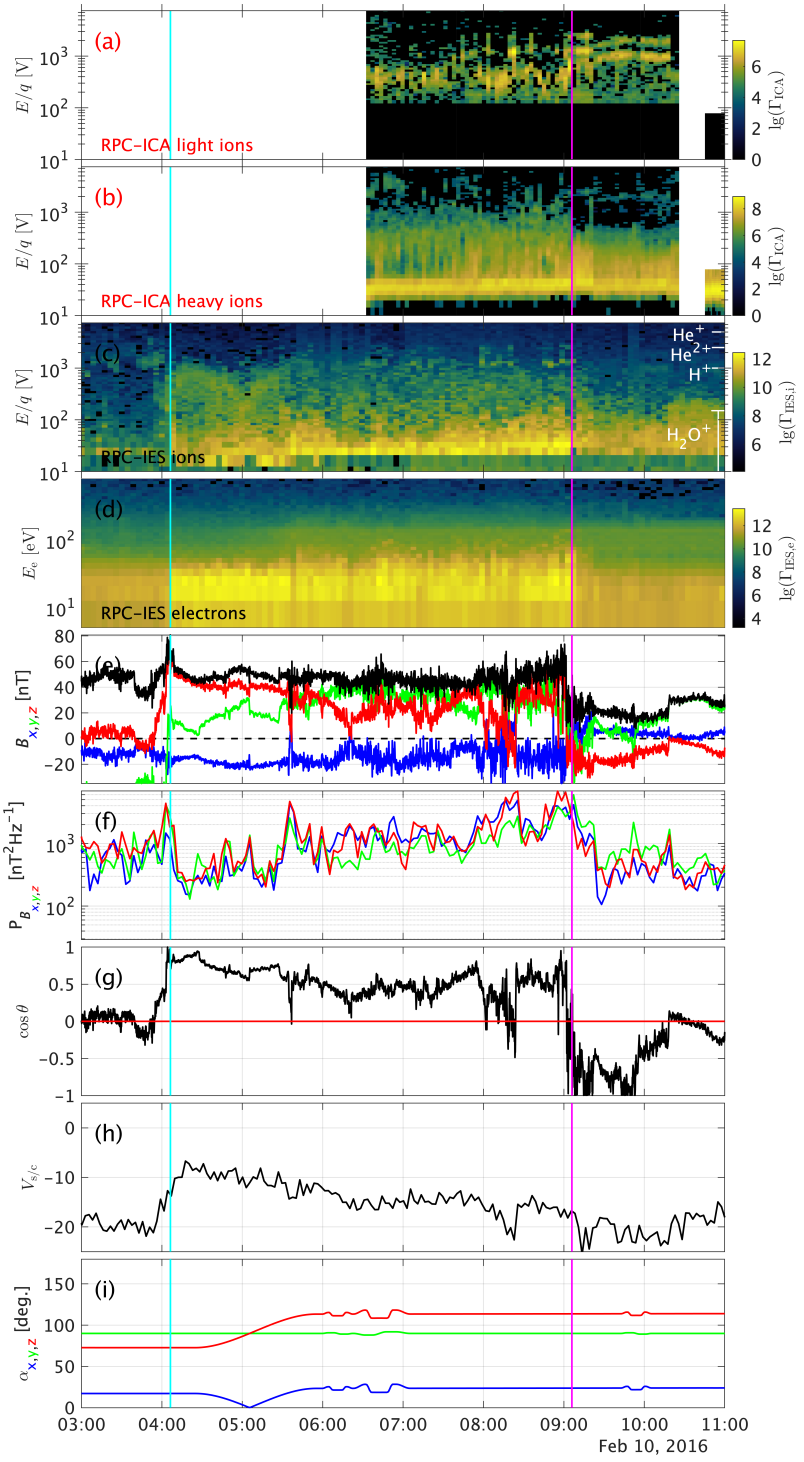

Figure 6. Observations of the event on February 10th, 2016. From top to bottom: a) ICA solar wind ions, b) ICA heavy ions, c) IES ions, d) IES electrons, e) magnetic field in CSEQ coordinates, f) magnetic power spectral density in the frequency range between 2 mHz and 15 mHz, g) angle between spacecraft position and convective electric field, and h) spacecraft attitude.

https://doi.org/10.5194/angeo-2020-66
Preprint. Discussion started: 16 October 2020


Annales Geophysicae Discussions

We present here also for the first time the spacecraft potential measurements for this boundary. We find that the spacecraft potential, and by extension the density of the plasma does not change significantly at the boundary. This was expected, as the plasma density at 67P at this point is dominated by the heavy ions and not the solar wind. Thus, the solar wind has only very little influence on the plasma density.

From the observations, we learn that the warm protons are mostly found in the ($+y$,$+E_c$) quadrant in a solar wind convective electric field frame. We can compare this to Hybrid simulations of the plasma environment at similar gas production rates (Lindkvist et al., 2018). Fig. 5 shows the proton density and flux (arrows) in a hybrid simulation. For a detailed description of the simulations and the input conditions used see Lindkvist et al. (2018) and Gunell et al. (2018). The infant bow shock as identified in the previous study is visible as the large asymmetric region of enhanced proton density. The purple box shows the approximate region that Rosetta was able to measure in. The simulation reveals a more detailed structure than a simple test particle picture. For example, the proton density enhancement in the upper left corner as well as the secondary IBS structure are due to the gyration of the protons. As the protons are accelerated by the electric field their trajectories form cycloids. In these two regions many of these cycloidal trajectories reach their cusps where the velocity is low, thus giving a higher density (see also Behar et al., 2018, upper panel in Fig. 7). A similar overshoot for the magnetic field has also been seen in simulations (upper left panel of Fig. 1 Lindkvist et al., 2018).

This structure is seen to extend farther into the $-E_c$ than the $+E_c$ hemisphere. However, it is also seen in Fig. 5 that the box showing the area covered by Rosetta barely reaches the IBS in that hemisphere. Instead we would actually expect to observe events in the $+E_c$ hemisphere. This is what is also seen in the observations shown in the right panel of Fig. 4. We have said above that the plasma and boundaries in it, such as the IBS, are necessarily non-stationary for Rosetta to be able to observe them. Nevertheless, a picture emerges of a plasma that is structured much like the stationary images obtained from the simulation results, but with deformation and translation of the structure being driven by changes in the solar wind.

Despite searching the entire dataset for which proton data is available, most events are found at intermediate gas production rates (see Fig. 3), but where we do observe higher gas production rates, the warm protons are observed further from the nucleus than for low gas production rates. The IBS is a structure that was speculated to form only at intermediate gas production rates, where the mass-loading is sufficient to slow down the solar wind, but not significant enough to form a large bow shock. Thus the IBS location does agree with our findings for warm protons.

We have made attempts to conclusively show that this structure is indeed a shock in the fluid dynamics sense. However, the plasma environment of the comet is far from a single fluid MHD plasma where the Rankine-Hugoniot conditions could be used to investigate the transition. For our situation, multi-ion and kinetic scale effects need to be accounted for. Motschmann et al. (1991a, b) derive multi-fluid R-H conditions and investigate the consequences of the second ion population on the behaviour of both ion flows at the shock. Fahr and Siewert (2015) show that including the kinetic effects from a multi-ion plasma changes the R-H conditions. They also found that the two ion populations can have a different behaviour when crossing the shock, for example the protons are still supersonic downstream of the shock, while the electrons and pick up ions are not. This demonstrates the complexity of multi-ion shocks. This seems to be the case here as well. While the solar wind ions are shocked, the plasma density used here is derived from electron densities which are a mixture of solar wind electrons and photoelectrons.

https://doi.org/10.5194/angeo-2020-66
Preprint. Discussion started: 16 October 2020


Annales Geophysicae Discussions

Thus, the overall plasma density does not change at the shock, which means that for the calculation of the R-H conditions one should actually use an estimate of the solar wind ion density instead. Unfortunately this is not available. The proton density estimate from ICA shows a large scatter, of which some may be an instrumental effect thus we cannot use the data to test the shock conditions. Most models of shock assume that the shock is in a stationary state. As already mentioned above, this is not the case for the observations with Rosetta, because to observe the transition the shock needs to move over the spacecraft and thus is not in a stationary state.

Behar et al. (2017) reported similar features in the ICA data as those used for our event detection. They made an attempt to describe the observations with a simple ion test particle picture. The model produces results similar to those of the hybrid simulations and fits with the deflection of the solar wind ions. It predicts a “caustic" as the boundary between the solar wind ion cavity and the solar wind dominated plasma. Our study concerns a similar structure, but we investigate here for the first time, the response of the plasma to such a change in the proton energy and thus broadens our understanding of the plasma. Although the test particle description agrees well with the observations of the ions, it does not explain the heating of the ions and electrons. This is expected for a model that does not include the feedback of the particle motion on the fields. However, it is entirely possible that those events that do not exhibit heating of the electrons are more similar to a model that treats the ions only as test particles with little influence on the behaviour of the plasma, while still including both electric and magnetic fields.

In future research, simultaneous observations at multiple points in space (Götz et al., 2019) would be a major advance in the ability to distinguish spatial and temporal dependence, and it is a necessity in assessing the stationarity or non-stationarity of the infant bow shock. ESA’s new F-class mission, Comet Interceptor, will be the first mission to provide multi-point measurements needed for this (Snodgrass and Jones, 2019). In hybrid simulations, the IBS response to solar wind variability could both shed light on the physics of cometary–solar wind interaction and aid in the interpretation of spacecraft data. There is, however, a vast range of cometary and solar wind parameters that must be sampled to obtain a complete picture. To understand the microphysics of shocks in general and infant bow shocks in particular one must also progress from hybrid simulations to simulations that accurately model electrons as well as ions. To address the microphysics, using spacecraft-based instruments, it is likewise important to resolve electron scales, both temporal and spatial.

5 Conclusions

We have expanded the previous study of the infant bow shock (Gunell et al., 2018) by searching for intervals with warm protons in the plasma around 67P. We first examined 13 cases in detail, and we have performed a statistical study of the whole Rosetta dataset. The results from both are similar. On average, the electron flux is increased in the downstream region, while the magnetic field magnitude decreases, and the magnetic field power spectral density and the density proxy increase. All parameters, except for the magnetic field magnitude, behave according to what was defined for the infant bow shock. About 10% of all events identified here behave exactly as expected for the IBS. Since the Rosetta spacecraft moved at speeds of only approximately $1\,\mathrm{m\,s^{-1}}$, it is only when the infant bow shock reacts to changes in the upstream plasma that the spacecraft crosses it. Our large statistical dataset therefore includes observations not only of IBS crossings but also detections of shocked

https://doi.org/10.5194/angeo-2020-66
Preprint. Discussion started: 16 October 2020


Annales Geophysicae Discussions

plasma downstream of the IBS itself, which nevertheless confirms its presence upstream of the spacecraft position. We therefore conclude that these warm protons are associated with the IBS in a very non-stationary plasma.

Most detections took place between $Q = 10^{26}\,\mathrm{s}^{-1}$ and $Q = 6 \times 10^{27}\,\mathrm{s}^{-1}$, which approximately corresponds to heliocentric distances between $1.7\,\mathrm{AU}$ and $2.7\,\mathrm{AU}$. It was observed preferentially in the $+E_c$ hemisphere due to its asymmetry.

While the precise nature of the IBS and the physics causing its formation remain to be revealed in future studies, we conclude that it is an asymmetric structure with many shock-like traits that is observed persistently during intermediate outgassing conditions. It is the infant bow shock that develops into the ordinary bow shock as the comet moves closer to the Sun and the outgassing increases further. This observation demonstrates again the uniqueness of the laboratory that the cometary environment can provide for the larger scope of plasma physics.

Data availability. Datasets of the RPC and ROSINA instruments onboard Rosetta are available at the ESA Planetary Science Archive (http://archives.esac.esa.int/psa Besse et al., 2018).

Appendix A: Additional events

Author contributions. CG performed the analysis and selection of intervals in collaboration with HG. HN contributed the interpretation of the ICA observations, KL that of the IES observations, FJ that of the LAP observations. KHG and MGGTT contributed on the interpretation of the results. All authors contributed to the writing of the final manuscript as well as the interpretation of the data.

Competing interests. None of the authors have any competing interests.

Acknowledgements. Part of this work was supported by the DLR project number 50 QP 1401. CG is supported by an ESA Research Fellowship. HG was supported by the Swedish National Space Agency grant 108/18 and by the Belgian Science Policy Office through the Solar-Terrestrial Centre of Excellence. Datasets of the RPC and ROSINA instruments onboard Rosetta are available at the ESA Planetary Science Archive (http://archives.esac.esa.int/psa Besse et al., 2018).

https://doi.org/10.5194/angeo-2020-66
Preprint. Discussion started: 16 October 2020

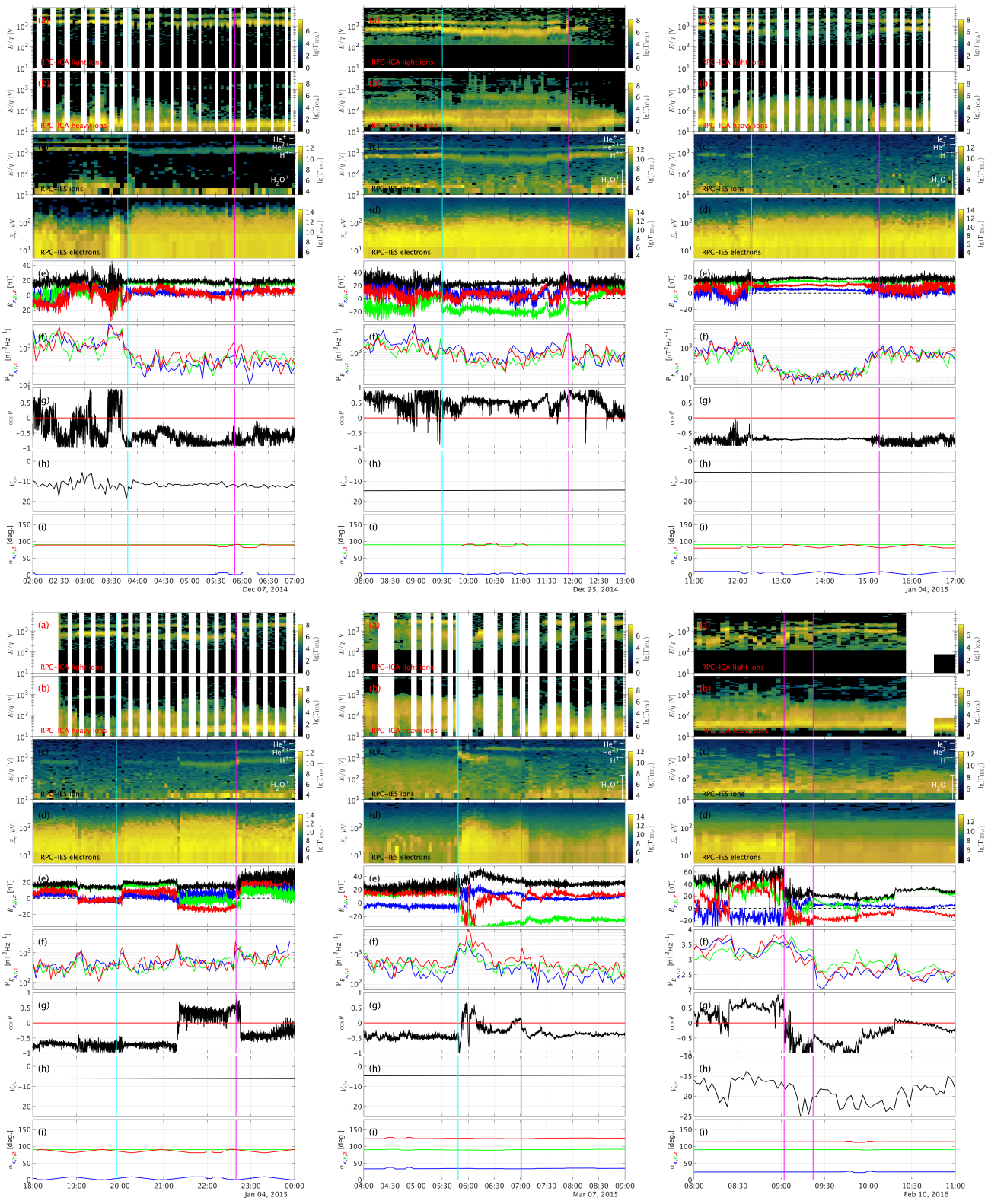

Figure A1. Observations of the plasma for the events shown in Table 1. Format is the same as in Figure 1.

https://doi.org/10.5194/angeo-2020-66
Preprint. Discussion started: 16 October 2020

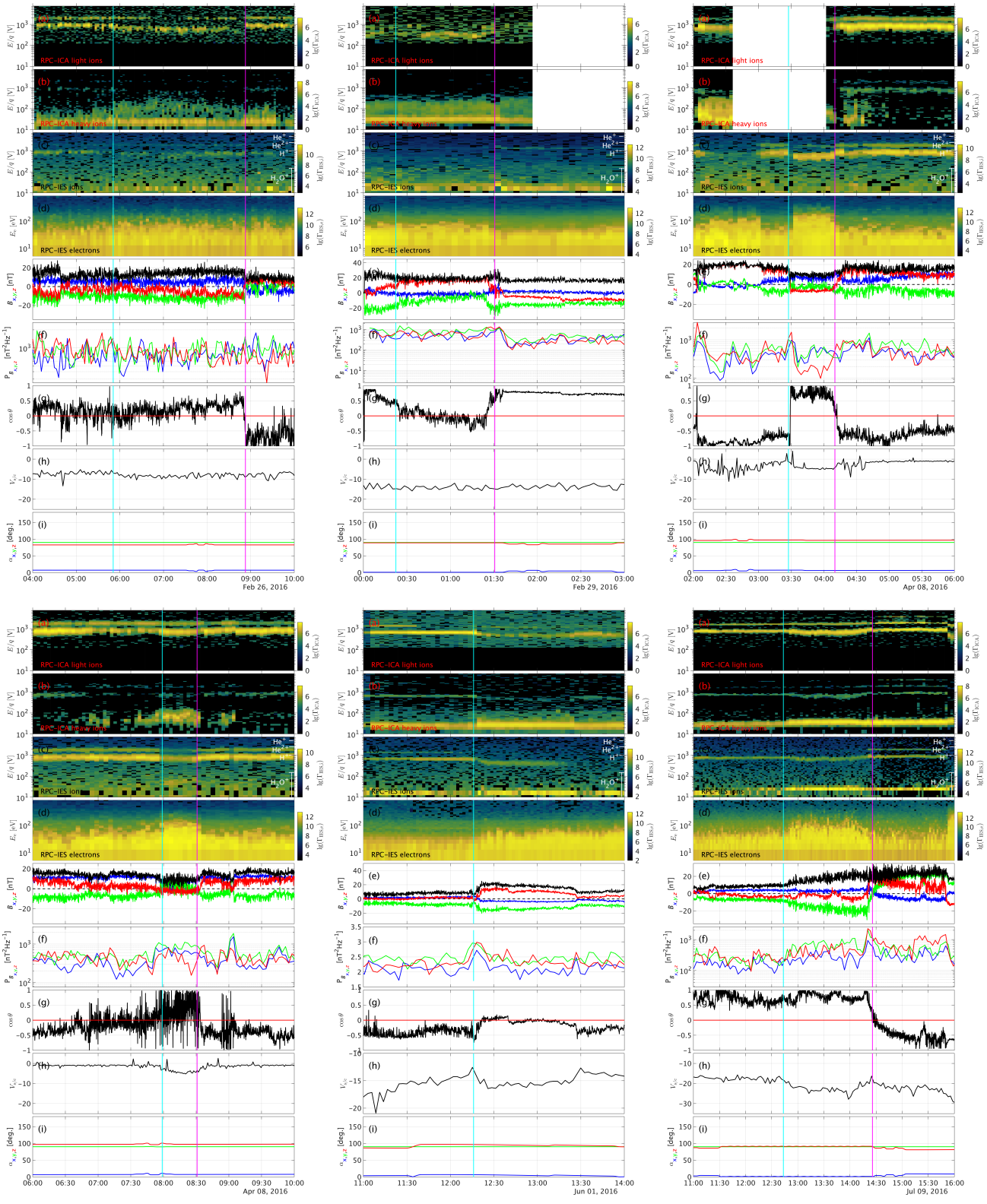

Figure A2. Observations of the plasma for the events shown in Table 1. Format is the same as in Figure 1.

https://doi.org/10.5194/angeo-2020-66
Preprint. Discussion started: 16 October 2020

Annales Geophysicae Discussions

References

Balogh, A. and Treumann, R. A.: Physics of Collisionless Shocks, vol. 12 of *ISSI Scientific Report Series*, Springer, New York, NY, https://doi.org/10.1007/978-1-4614-6099-2, 2013.

Balsiger, H., Altwegg, K., Bochsler, P., Eberhardt, P., Fischer, J., Graf, S., Jäckel, A., Kopp, E., Langer, U., Mildner, M., Müller, J., Riesen, T., Rubin, M., Scherer, S., Wurz, P., Wüthrich, S., Arijs, E., Delanoye, S., De Keyser, J., Neefs, E., Nevejans, D., Rème, H., Aoustin, C., Mazelle, C., Médale, J.-L., Sauvaud, J. A., Berthelier, J.-J., Bertaux, J.-L., Duvet, L., Illiano, J.-M., Fuselier, S. A., Ghielmetti, A. G., Magoncelli, T., Shelley, E. G., Korth, A., Heerlein, K., Lauche, H., Livi, S., Loose, A., Mall, U., Wilken, B., Gliem, F., Fiethe, B., Gombosi, T. I., Block, B., Carignan, G. R., Fisk, L. A., Waite, J. H., Young, D. T., and Wollnik, H.: Rosina Rosetta Orbiter Spectrometer for Ion and Neutral Analysis, Space Science Reviews, 128, 745–801, https://doi.org/10.1007/s11214-006-8335-3, 2007.

Behar, E., Nilsson, H., Alho, M., Goetz, C., and Tsurutani, B.: The birth and growth of a solar wind cavity around a comet - Rosetta observations, MNRAS, 469, S396–S403, https://doi.org/10.1093/mnras/stx1871, 2017.

Behar, E., Tabone, B., Saillenfest, M., Henri, P., Deca, J., Lindkvist, J., Holmström, M., and Nilsson, H.: A global 2D analytical model of the solar wind dynamics around a comet., Astronomy & Astrophysics, https://doi.org/10.1051/0004-6361/201832736, 2018.

Besse, S., Vallat, C., Barthelemy, M., Coia, D., Costa, M., De Marchi, G., Fraga, D., Grotheer, E., Heather, D., Lim, T., Martinez, S., Arviset, C., Barbarisi, I., Docasal, R., Macfarlane, A., Rios, C., Saiz, J., and Vallejo, F.: ESA's Planetary Science Archive: Preserve and present reliable scientific data sets, Planet. Space Sci., 150, 131–140, https://doi.org/10.1016/j.pss.2017.07.013, 2018.

Biermann, L., Brosowski, B., and Schmidt, H. U.: The interactions of the solar wind with a comet, Solar Physics, 1, 254–284, https://doi.org/10.1007/BF00150860, 1967.

Breuillard, H., Henri, P., Bucciantini, L., Volwerk, M., Karlsson, T., Eriksson, A., Johansson, F., Odelstad, E., Richter, I., Goetz, C., Vallières, X., and Hajra, R.: The properties of the singing comet waves in the 67P/Churyumov–Gerasimenko plasma environment as observed by the Rosetta mission, A&A, https://doi.org/10.1051/0004-6361/201834876, 2019.

Burch, J. L., Goldstein, R., Cravens, T. E., Gibson, W. C., Lundin, R. N., Pollock, C. J., Winningham, J. D., and Young, D. T.: RPC-IES: The Ion and Electron Sensor of the Rosetta Plasma Consortium, Space Sci. Rev., 128, 697–712, https://doi.org/10.1007/s11214-006-9002-4, 2007.

Carr, C., Cupido, E., Lee, C. G. Y., Balogh, A., Beek, T., Burch, J. L., Dunford, C. N., Eriksson, A. I., Gill, R., Glassmeier, K. H., Goldstein, R., Lagoutte, D., Lundin, R., Lundin, K., Lybekk, B., Michau, J. L., Musmann, G., Nilsson, H., Pollock, C., Richter, I., and Trotignon, J. G.: RPC: The Rosetta Plasma Consortium, Space Sci. Rev., 128, 629–647, https://doi.org/10.1007/s11214-006-9136-4, 2007.

Deca, J., Divin, A., Henri, P., Eriksson, A., Markidis, S., Olshevsky, V., and Horányi, M.: Electron and Ion Dynamics of the Solar Wind Interaction with a Weakly Outgassing Comet, Phys. Rev. Lett., 118, 205101, https://doi.org/10.1103/PhysRevLett.118.205101, 2017.

Edberg, N. J. T., Eriksson, A. I., Odelstad, E., Vigren, E., Andrews, D. J., Johansson, F., Burch, J. L., Carr, C. M., Cupido, E., Glassmeier, K.-H., Goldstein, R., Halekas, J. S., Henri, P., Koenders, C., Mandt, K., Mokashi, P., Nemeth, Z., Nilsson, H., Ramstad, R., Richter, I., and Wieser, G. S.: Solar wind interaction with comet 67P: Impacts of corotating interaction regions, Journal of Geophysical Research (Space Physics), 121, 949–965, https://doi.org/10.1002/2015JA022147, 2016.

Edberg, N. J. T., Eriksson, A. I., Vigren, E., Johansson, F. L., Goetz, C., Nilsson, H., Gilet, N., and Henri, P.: The Convective Electric Field Influence on the Cold Plasma and Diamagnetic Cavity of Comet 67P, AJ, 158, 71, https://doi.org/10.3847/1538-3881/ab2d28, 2019.

https://doi.org/10.5194/angeo-2020-66
Preprint. Discussion started: 16 October 2020

Eriksson, A. I., Boström, R., Gill, R., Åhlén, L., Jansson, S.-E., Wahlund, J.-E., André, M., Mälkki, A., Holtet, J. A., Lybekk, B., Pedersen, A., and Blomberg, L. G.: RPC-LAP: The Rosetta Langmuir Probe Instrument, Space Science Reviews, 128, 729–744, https://doi.org/10.1007/s11214-006-9003-3, 2007.

Fahr, H. J. and Siewert, M.: Entropy generation at multi-fluid magnetohydrodynamic shocks with emphasis to the solar wind termination shock, A&A, 576, A100, https://doi.org/10.1051/0004-6361/201424485, 2015.

Flammer, K. R. and Mendis, D. A.: A note on the mass-loaded MHD flow of the solar wind towards a cometary nucleus, Ap&SS, 182, 155–162, https://doi.org/10.1007/BF00646450, 1991.

Glassmeier, K.-H.: Interaction of the solar wind with comets: A Rosetta perspective, Philosophical Transactions of the Royal Astronomical Society A, 375, 20160 256, https://doi.org/10.1098/rsta.2016.0256, 2017.

Glassmeier, K.-H., Boehnhardt, H., Koschny, D., Kührt, E., and Richter, I.: The Rosetta Mission: Flying Towards the Origin of the Solar System, Space Science Reviews, 128, 1–21, https://doi.org/10.1007/s11214-006-9140-8, 2007a.

Glassmeier, K.-H., Richter, I., Diedrich, A., Musmann, G., Auster, U., Motschmann, U., Balogh, A., Carr, C., Cupido, E., Coates, A., Rother, M., Schwingenschuh, K., Szegö, K., and Tsurutani, B.: RPC-MAG The Fluxgate Magnetometer in the ROSETTA Plasma Consortium, Space Science Reviews, 128, 649–670, https://doi.org/10.1007/s11214-006-9114-x, 2007b.

Goetz, C., Koenders, C., Hansen, K. C., Burch, J., Carr, C., Eriksson, A., Frühauff, D., Güttler, C., Henri, P., Nilsson, H., Richter, I., Rubin, M., Sierks, H., Tsurutani, B., Volwerk, M., and Glassmeier, K. H.: Structure and evolution of the diamagnetic cavity at comet 67P/Churyumov-Gerasimenko, MNRAS, 462, S459–S467, https://doi.org/10.1093/mnras/stw3148, 2016.

Goetz, C., Volwerk, M., Richter, I., and Glassmeier, K.-H.: Evolution of the magnetic field at comet 67P/Churyumov-Gerasimenko, MNRAS, 469, S268–S275, https://doi.org/10.1093/mnras/stx1570, 2017.

Götz, C., Gunell, H., Volwerk, M., Beth, A., Eriksson, A., Galand, M., Henri, P., Nilsson, H., Wedlund, C. S., Alho, M., Andersson, L., Andre, N., De Keyser, J., Deca, J., Ge, Y., Glaßmeier, K.-H., Hajra, R., Karlsson, T., Kasahara, S., Kolmasova, I., LLera, K., Madanian, H., Mann, I., Mazelle, C., Odelstad, E., Plaschke, F., Rubin, M., Sanchez-Cano, B., Snodgrass, C., and Vigren, E.: Cometary Plasma Science – A White Paper in response to the Voyage 2050 Call by the European Space Agency, arXiv e-prints, arXiv:1908.00377, 2019.

Gunell, H., Goetz, C., Simon Wedlund, C., Lindkvist, J., Hamrin, M., Nilsson, H., Llera, K., Eriksson, A., and Holmström, M.: The infant bow shock: a new frontier at a weak activity comet, A&A, 619, L2, https://doi.org/10.1051/0004-6361/201834225, 2018.

Gunell, H., Lindkvist, J., Goetz, C., Nilsson, H., and Hamrin, M.: Polarisation of a small-scale cometary plasma environment: Particle-in-cell modelling of comet 67P/Churyumov-Gerasimenko, Astronomy & Astrophysics, 631, A174, https://doi.org/10.1051/0004-6361/201936004, 2019.

Hall, B. E. S., Lester, M., Sánchez-Cano, B., Nichols, J. D., Andrews, D. J., Edberg, N. J. T., Opgenoorth, H. J., Fränz, M., Holmström, M., Ramstad, R., Witasse, O., Cartacci, M., Cicchetti, A., Noschese, R., and Orosei, R.: Annual variations in the Martian bow shock location as observed by the Mars Express mission, J. Geophys. Res. (Space Physics), 121, https://doi.org/10.1002/2016JA023316, 2016.

Haser, L.: Distribution d'intensité dans la tête d'une comète, Bulletin de la Societe Royale des Sciences de Liege, 43, 740–750, 1957.

Hässig, M., Altwegg, K., Balsiger, H., Bar-Nun, A., Berthelier, J. J., Bieler, A., Bochsler, P., Briois, C., Calmonte, U., Combi, M., De Keyser, J., Eberhardt, P., Fiethe, B., Fuselier, S. A., Galand, M., Gasc, S., Gombosi, T. I., Hansen, K. C., Jäckel, A., Keller, H. U., Kopp, E., Korth, A., Kührt, E., Le Roy, L., Mall, U., Marty, B., Mousis, O., Neefs, E., Owen, T., Rème, H., Rubin, M., Sémon, T., Tornow, C., Tzou, C.-Y., Waite, J. H., and Wurz, P.: Time variability and heterogeneity in the coma of 67P/Churyumov-Gerasimenko, Science, 347, aaa0276, https://doi.org/10.1126/science.aaa0276, 2015.

https://doi.org/10.5194/angeo-2020-66
Preprint. Discussion started: 16 October 2020

Koenders, C., Glassmeier, K.-H., Richter, I., Motschmann, U., and Rubin, M.: Revisiting cometary bow shock positions, Planetary and Space Science, 87, 85–95, https://doi.org/10.1016/j.pss.2013.08.009, 2013.

Koenders, C., Goetz, C., Richter, I., Motschmann, U., and Glassmeier, K.-H.: Magnetic field pile-up and draping at intermediately active comets: results from comet 67P/Churyumov-Gerasimenko at 2.0 AU, MNRAS, 462, S235–S241, https://doi.org/10.1093/mnras/stw2480, 2016a.

Koenders, C., Perschke, C., Goetz, C., Richter, I., Motschmann, U., and Glassmeier, K. H.: Low-frequency waves at comet 67P/Churyumov-Gerasimenko. Observations compared to numerical simulations, A&A, 594, A66, https://doi.org/10.1051/0004-6361/201628803, 2016b.

Lavraud, B. and Larson, D. E.: Correcting moments of in situ particle distribution functions for spacecraft electrostatic charging, Journal of Geophysical Research (Space Physics), 121, 8462–8474, https://doi.org/10.1002/2016JA022591, 2016.

Lindkvist, J., Hamrin, M., Gunell, H., Nilsson, H., Simon Wedlund, C., Kallio, E., Mann, I., Pitkänen, T., and Karlsson, T.: Energy conversion in cometary atmospheres Hybrid modeling of 67P/Churyumov-Gerasimenko, Astronomy & Astrophysics, 616, A81, https://doi.org/10.1051/0004-6361/201732353, 2018.

Madanian, H., Burch, J. L., Eriksson, A. I., Cravens, T. E., Galand, M., Vigren, E., Goldstein, R., Nemeth, Z., Mokashi, P., Richter, I., and Rubin, M.: Electron dynamics near diamagnetic regions of comet 67P/Churyumov- Gerasimenko, Planet. Space Sci., 187, 104924, https://doi.org/10.1016/j.pss.2020.104924, 2020.

Maggiolo, R., Hamrin, M., De Keyser, J., Pitkänen, T., Cessateur, G., Gunell, H., and Maes, L.: The Delayed Time Response of Geomagnetic Activity to the Solar Wind, Journal of Geophysical Research (Space Physics), 122, 11,109–11,127, https://doi.org/10.1002/2016JA023793, 2017.

Mandt, K. E., Eriksson, A., Edberg, N. J. T., Koenders, C., Broiles, T., Fuselier, S. A., Henri, P., Nemeth, Z., Alho, M., Biver, N., Beth, A., Burch, J., Carr, C., Chae, K., Coates, A. J., Cupido, E., Galand, M., Glassmeier, K.-H., Goetz, C., Goldstein, R., Hansen, K. C., Haiducek, J., Kallio, E., Lebreton, J.-P., Luspay-Kuti, A., Mokashi, P., Nilsson, H., Opitz, A., Richter, I., Samara, M., Szego, K., Tzou, C.-Y., Volwerk, M., Simon Wedlund, C., and Stenberg Wieser, G.: RPC observation of the development and evolution of plasma interaction boundaries at 67P/Churyumov-Gerasimenko, MNRAS, 462, S9–S22, https://doi.org/10.1093/mnras/stw1736, 2016.

Martinecz, C., Fränz, M., Woch, J., Krupp, N., Roussos, E., Dubinin, E., Motschmann, U., Barabash, S., Lundin, R., Holmström, M., Andersson, H., Yamauchi, M., Grigoriev, A., Futaana, Y., Brinkfeldt, K., Gunell, H., Frahm, R. A., Winningham, J. D., Sharber, J. R., Scherrer, J., Coates, A. J., Linder, D. R., Kataria, D. O., Kallio, E., Sales, T., Schmidt, W., Riihela, P., Koskinen, H. E. J., Kozyra, J. U., Luhmann, J., Russell, C. T., Roelof, E. C., Brandt, P., Curtis, C. C., Hsieh, K. C., Sandel, B. R., Grande, M., Sauvaud, J.-A., Fedorov, A., Thocaven, J.-J., Mazelle, C., McKenna-Lawler, S., Orsini, S., Cerulli-Irelli, R., Maggi, M., Mura, A., Milillo, A., Wurz, P., Galli, A., Bochsler, P., Asamura, K., Szego, K., Baumjohann, W., Zhang, T. L., and Lammer, H.: Location of the bow shock and ion composition boundaries at Venus—initial determinations from Venus Express ASPERA-4, Planet. Space Sci., 56, 780–784, https://doi.org/10.1016/j.pss.2007.07.007, 2008.

Motschmann, U., Sauer, K., Roatsch, T., and McKenzie, J. F.: Multiple-ion plasma boundaries, Advances in Space Research, 11, 69–72, https://doi.org/10.1016/0273-1177(91)90013-A, 1991a.

Motschmann, U., Sauer, K., Roatsch, T., and McKenzie, J. F.: Subcritical multiple-ion shocks, J. Geophys. Res., 96, 13 841–13 848, https://doi.org/10.1029/91JA00638, 1991b.

Neubauer, F. M., Glassmeier, K. H., Pohl, M., Raeder, J., Acuña, M. H., Burlaga, L. F., Ness, N. F., Musmann, G., Mariani, F., Wallis, M. K., Ungstrup, E., and Schmidt, H. U.: First results from the Giotto magnetometer experiment at comet Halley, Nature, 321, 352–355, https://doi.org/10.1038/321352a0, 1986.

https://doi.org/10.5194/angeo-2020-66
Preprint. Discussion started: 16 October 2020

Nilsson, H., Lundin, R., Lundin, K., Barabash, S., Borg, H., Norberg, O., Fedorov, A., Sauvaud, J.-A., Koskinen, H., Kallio, E., Riihelä, P., and Burch, J. L.: RPC-ICA: The Ion Composition Analyzer of the Rosetta Plasma Consortium, Space Sci. Rev., 128, 671–695, https://doi.org/10.1007/s11214-006-9031-z, 2007.

Nilsson, H., Stenberg Wieser, G., Behar, E., Gunell, H., Galand, M., Simon Wedlund, C., Alho, M., Goetz, C., Yamauchi, M., Henri, P., and Eriksson, E. O. A.: Evolution of the ion environment of comet 67P during the Rosetta mission as seen by RPC-ICA, Monthly Notices of the Royal Astronomical Society, 469, S252–S261, https://doi.org/10.1093/mnras/stx1491, 2017.

Nilsson, H., Gunell, H., Karlsson, T., Brenning, N., Henri, P., Goetz, C., Eriksson, A. I., Behar, E., Stenberg Wieser, G., and Vallières, X.: Size of a plasma cloud matters: The polarisation electric field of a small-scale comet ionosphere, Astronomy & Astrophysics, 616, A50, https://doi.org/10.1051/0004-6361/201833199, 2018.

Odelstad, E., Eriksson, A. I., Edberg, N. J. T., Johansson, F., Vigren, E., André, M., Tzou, C. Y., Carr, C., and Cupido, E.: Evolution of the plasma environment of comet 67P from spacecraft potential measurements by the Rosetta Langmuir probe instrument, Geophysical Research Letters, 42, 10 126–10 134, https://doi.org/10.1002/2015GL066599, 2015.

Simon Wedlund, C., Alho, M., Gronoff, G., Kallio, E., Gunell, H., Nilsson, H., Lindkvist, J., Behar, E., Stenberg Wieser, G., and Miloch, W. J.: Hybrid modelling of cometary plasma environments. I. Impact of photoionisation, charge exchange, and electron ionisation on bow shock and cometopause at 67P/Churyumov-Gerasimenko, A&A, 604, A73, https://doi.org/10.1051/0004-6361/201730514, 2017.

Simon Wedlund, C., Behar, E., Nilsson, H., Alho, M., Kallio, E., Gunell, H., Bodewits, D., Heritier, K., Galand, M., Beth, A., Rubin, M., Altwegg, K., Volwerk, M., Gronoff, G., and Hoekstra, R.: Solar wind charge exchange in cometary atmospheres III. Results from the Rosetta mission to comet 67P/Churyumov-Gerasimenko, Astronomy & Astrophysics, https://doi.org/10.1051/0004-6361/201834881, 2019.

Snodgrass, C. and Jones, G. H.: The European Space Agency's Comet Interceptor lies in wait, Nature Communications, 10, 5418, https://doi.org/10.1038/s41467-019-13470-1, 2019.

Trotignon, J. G., Michau, J. L., Lagoutte, D., Chabassière, M., Chalumeau, G., Colin, F., Décréau, P. M. E., Geiswiller, J., Gille, P., Grard, R., Hachemi, T., Hamelin, M., Eriksson, A., Laakso, H., Lebreton, J. P., Mazelle, C., Randriamboarison, O., Schmidt, W., Smit, A., Telljohann, U., and Zamora, P.: RPC-MIP: the Mutual Impedance Probe of the Rosetta Plasma Consortium, Space Sci. Rev., 128, 713–728, https://doi.org/10.1007/s11214-006-9005-1, 2007.

Ziegler, H. J. and Schindler, K.: Structure of subcritical perpendicular shock waves, The Physics of Fluids, 31, 570–576, https://doi.org/10.1063/1.866839, 1988.